Rapid Communications | Editors' Suggestion

Topological magnons in Kitaev magnets at high fields

P. A. McClarty,[1] X.-Y. Dong,[1] M. Gohlke,[1] J. G. Rau,[1] F. Pollmann,[2] R. Moessner,[1] and K. Penc[1,3,4]

[1]*Max Planck Institute for the Physics of Complex Systems, Nöthnitzer Strasse 38, D-01187 Dresden, Germany*

[2]*Physics Department, Technical University Munich, James-Franck-Strasse 1, D-85748 Garching, Germany*

[3]*Institute for Solid State Physics and Optics, Wigner RCP, P.O. Box 49, H-1525 Budapest, Hungary*

[4]*Department of Physics, Budapest University of Technology and Economics and MTA-BME Lendület Magneto-optical Spectroscopy Research Group, 1111 Budapest, Hungary*

(Received 14 February 2018; published 7 August 2018)

We study the Kitaev-Heisenberg Γ-Γ′ model that describes the magnetism in spin-orbit coupled honeycomb lattice Mott insulators. In strong magnetic fields perpendicular to the plane of the lattice ([111] direction) that bring the system into the fully polarized paramagnetic phase, we find that the spin-wave bands carry nontrivial Chern numbers over large regions of the phase diagram, implying the presence of chiral magnon edge states. In contrast to other topological magnon systems, the topological nontriviality of these systems results from the presence of anisotropic terms in the Hamiltonian that do not conserve the number of magnons. Since the effects of interactions are suppressed by the exchange scale divided by the applied field strength, the validity of the single-particle picture is tunable, making paramagnetic phases particularly suitable for the exploration of this physics. Using time-dependent density matrix renormalization group methods and interacting spin-wave theory, we demonstrate the presence of the chiral edge mode and its evolution with field.

DOI: 10.1103/PhysRevB.98.060404

There have been few ideas more fertile in recent condensed matter physics than the notion that band structures in solids may carry nontrivial topological indices which determine and protect certain properties of the spectrum of the solid at interfaces [1,2]. The core idea, formulated in the context of the integer quantum Hall effect, has led to a proliferation of novel topological states of matter including topological insulators protected by time-reversal or by crystalline symmetries, as well as Weyl and Dirac semimetals [3,4], many of which have been realized in the laboratory. Analogs of this physics have been explored in photonic crystals [5], in the mechanical properties of metamaterials [6], and even in atmospheric physics [7].

The concepts underlying electronic topological insulators have potentially very interesting ramifications for our understanding of magnetic materials. For example, sharp magnon bands where they exist in two-dimensional ordered magnets may carry nonzero Chern number with the consequence that there are topologically protected spin waves at the edge of the system with a net chirality. A handful of models have been proposed that realize such Chern bands [8–15]. There is experimental evidence that such models may be realized in real materials [14,16]. What has been lacking on the theoretical side is a clear demonstration that the chiral edge states can be robust in the presence of interactions between magnons.

In particular, one important feature that distinguishes electronic topological insulators from their bosonic analogs is that, in the latter, interactions are more likely to play an important role, possibly resulting in a breakdown of the single-particle picture. In the case of the kagome ferromagnet with Dzyaloshinskii-Moriya, it has been argued that magnon-magnon interactions broaden the bulk bands on a scale comparable to the bulk gap so that the band topology cannot be understood in terms of single magnons [17]. So the question remains open whether any model can be found in which the prediction of chiral edge modes in a magnonic band structure survives in the strong-coupling limit.

In this Rapid Communication, we propose a route to realizing topological magnon bands in systems of considerable current interest: honeycomb magnets with significant Kitaev exchange [18–43], some of which may be proximate to quantum spin-liquid phases [36,44,45]. The model we study has nonvanishing anomalous (number-nonconserving) terms in the quadratic spin-wave Hamiltonian and, in contrast to previous models of topological magnons, it is these terms that are responsible for opening up a gap in the spectrum leading to Chern bands. In addition, we present evidence that the chiral surface states that are present and topologically protected in linear spin-wave theory survive the presence of magnon-magnon interactions and hence should be experimentally detectable in principle. The key to accessing this is to field-tune the system into the paramagnetic phase so that multimagnon states are pushed to energies much higher than the single magnon states. Our time-dependent density matrix renormalization group (DMRG) results provide a nonperturbative demonstration of the robustness of the chiral edge mode

Model. We consider the Hamiltonian [30,46]

$$\mathcal{H} = J\sum_{\langle i,j\rangle}\mathbf{S}_i\cdot\mathbf{S}_j + \sum_{\langle i,j\rangle_\gamma}\left\{2K\mathrm{S}_i^\gamma\mathrm{S}_j^\gamma + \Gamma\left(\mathrm{S}_i^\alpha\mathrm{S}_j^\beta + \mathrm{S}_i^\beta\mathrm{S}_j^\alpha\right)\right\} - \boldsymbol{h}\cdot\sum_i\mathbf{S}_i, \tag{1}$$

where the indices $\{\alpha,\beta,\gamma\}$ run over components $\{x,y,z\}$ with the γ component corresponding to one of the three types of bond as indicated in Fig. 1(a) [see also the Supplemental Material (SM) [47]]. Models with significant K/J have

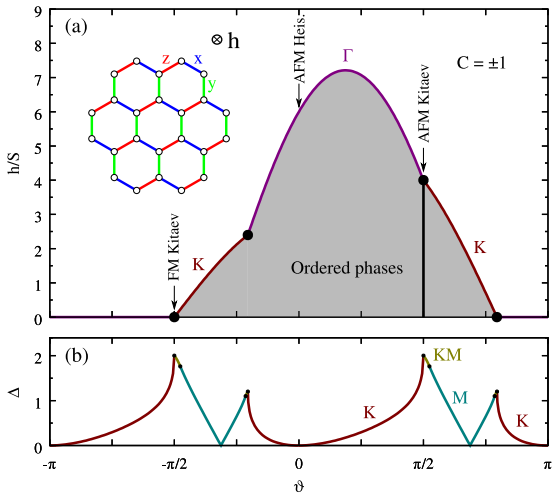

FIG. 1. (a) The phase diagram of the Kitaev-Heisenberg model as a function of ϑ and h/S as extracted from the spin-wave spectrum. The region of ordered phases is determined from the gap closure in the spin-wave spectrum while at the boundary of this region the corresponding ordering wave vector is indicated. The true semiclassical phase diagram has small regions, away from the Kitaev points, separated from the paramagnetic phase by first-order transitions (shown in Ref. [47]) and above the threshold field shown here which are not captured using our technique [34,35]. The rest of the phase diagram lies in the fully polarized phase. The entirety of the polarized paramagnetic region hosts topologically nontrivial magnons at the semiclassical level. Inset: Honeycomb lattice cluster with 24 sites. The different colored bonds correspond to the three types of coupling in the Kitaev model $\mathsf{S}_i^\gamma \mathsf{S}_j^\gamma$ for $\gamma = x$ (blue), y (green), and z (red) corresponding to the projections of the cubic axes onto the honeycomb plane. The [111] field direction, indicated on the figure, is perpendicular to the plane. The exact diagonalization results presented in this Rapid Communication were obtained for the Kitaev-Heisenberg model defined on this cluster. (b) shows the minimal gap between the spin-wave modes. The wave vector at which the gap is minimal is indicated by the color.

been proposed to underlie the correlated magnetism observed in the effective spin one-half systems $A_2\mathrm{IrO}_3$ ($A = \mathrm{Na,Li}$) [24–26,30,32,38,46] and α-RuCl_3 [29,33,36,41,48–50] following theoretical work that laid the basis for the possibility of large compass-type interactions in such honeycomb magnets [22,23]. A fourth exchange coupling Γ' is allowed by symmetry [30,46,47]. We postpone a discussion of the effects of the Γ and Γ' terms until later on and focus, for now, on the remaining Hamiltonian. We parametrize this Kitaev-Heisenberg model using an angle ϑ so that $J = \cos\vartheta$ and $K = \sin\vartheta$.

Noninteracting magnons. From now on, we consider the case where the magnetic field, of magnitude h, is applied parallel to [111] (Fig. 1). For h greater than some threshold, the moments are fully polarized in the field direction and we expand the moments in small fluctuations about this collinear state in Holstein-Primakoff bosons [51]. The quadratic Hamiltonian that results at order S is of the form $\mathcal{H}_{\mathrm{KH-LSW}} = \sum_{\boldsymbol{k}} \boldsymbol{\Upsilon}_{\boldsymbol{k}}^\dagger \mathbf{M}(\boldsymbol{k}) \boldsymbol{\Upsilon}_{\boldsymbol{k}}$, where $\boldsymbol{\Upsilon}_{\boldsymbol{k}} = (a_{\boldsymbol{k}}\ b_{\boldsymbol{k}}\ a_{-\boldsymbol{k}}^\dagger\ b_{-\boldsymbol{k}}^\dagger)^T$ with a and b bosons living on the two different honeycomb sublattices. The 4×4 Hamiltonian $\mathbf{M}(\boldsymbol{k})$, which is given explicitly in the SM, takes the form

$$\mathbf{M}(\boldsymbol{k}) = \begin{pmatrix} \mathsf{A}(\boldsymbol{k}) & \mathsf{B}(\boldsymbol{k}) \\ \mathsf{B}^\dagger(\boldsymbol{k}) & \mathsf{A}^T(-\boldsymbol{k}) \end{pmatrix}, \tag{2}$$

where the A block contains the number-conserving terms $a^\dagger a$, and B, which is proportional to coupling K, contains the number-nonconserving terms $a^\dagger a^\dagger$. The eigenproblem for this Hamiltonian, leading to two spin-wave branches $\omega_{\boldsymbol{k}}^\alpha$ for $\alpha = 1,2$, may be solved by performing a bosonic Bogoliubov transformation.

The phase diagram of the J-K model is shown in Fig. 1(a), indicating the fully polarized phase and regions of spontaneous magnetic order obtained by finding the couplings at which magnons condense—the translational symmetry of these phases is then determined by the condensation wave vector. The precise nature of the ordered states can be found in Refs. [34,35].

We first focus on the antiferromagnetic (AFM) Kitaev point $\vartheta = \pi/2$ ($J = 0$). The linear spin-wave dispersions along high-symmetry lines are shown in Fig. 2(a) for $h/S = 6$. For $h/S > 4$, the spectrum exhibits both a nonzero gap to the lowest mode and a gap between the modes. As $h/S \to 4$ the lowest mode falls to zero across the entire zone, corresponding to the onset of a classical spin-liquid regime, while the highest mode is completely gapped and dispersive.

Since the two bands do not touch at $\vartheta = \pi/2$, the Berry curvature is everywhere well defined (see SM [47]). The Chern numbers of the two bands at this coupling are ± 1 for all $h/S \geqslant 4$, implying the existence of chiral magnon edge modes. Since the bulk topology is not altered by modifications to the ground state in the vicinity of the boundary, we may illustrate the phenomenon with a linear spin-wave calculation of the spectrum above the collinear spin state on a slab geometry with zigzag boundaries parametrized by the momentum along the translation invariant direction. Such a calculation [47] reveals a pair of modes, each with a well-defined chirality, running between the bulk bands and with the weight of the wave function of these interband modes concentrated at opposite edges.

We may gain some insight into the mechanism that leads to the topological magnon bands. The $\vartheta = 0$ Hamiltonian ($K = 0$) has only number-conserving terms and the two magnon bands meet at the K point. Inspection of the Hamiltonian $\mathbf{M}(\boldsymbol{k})$ shows that the A block contains the two couplings only in the combination $J + \frac{2K}{3}$ so the number-nonconserving terms of the B block must be responsible for the gap opening between the bands in the magnon spectrum. These terms also break an effective time-reversal symmetry, leading to the identification of the magnon bands with the topological insulator class D [52].

The observation that the gap closes as $1/h$ at high fields suggests that further insight may be gained by carrying out a Schrieffer-Wolff transformation perturbatively in the anomalous terms to obtain an effective Hamiltonian in the number-conserving sector [47]. One finds to second order that the nearest-neighbor coupling is renormalized and effective second-neighbor hopping terms are generated that are of the same form as those arising from a bare second-neighbor Dzyaloshinskii-Moriya (DM) exchange coupling. In short, at very high fields, the spin-wave spectrum of the Kitaev model

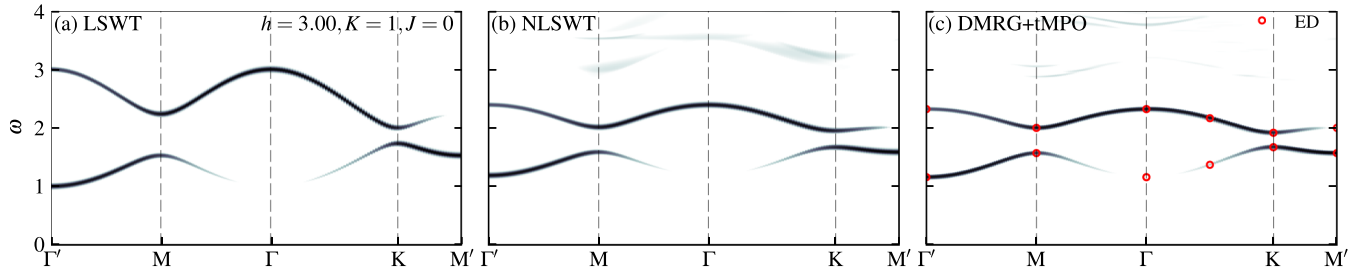

FIG. 2. Dynamical correlation function $S(\boldsymbol{k},\omega)$ computed along high-symmetry lines for $h = 3$ ($S = 1/2$) at the AFM Kitaev point $\vartheta = \pi/2$. The intensity scale is logarithmic from 5×10^{-3} to 1. (a) Linear spin-wave theory, (b) nonlinear spin-wave theory, and (c) time-dependent DMRG, all with Gaussian broadening of the lines for purposes of presentation $\sigma_\omega = 0.01$. The overlaid points in (c) show single magnon states obtained from 24-site ED with periodic boundary conditions.

reduces to that of a honeycomb ferromagnet with second-neighbor DM exchange that is known from earlier work to exhibit Chern bands [11].

We now consider the entire J-K semiclassical paramagnetic regime. The lower panel of Fig. 1(b) shows that the two magnon bands touch at four distinct ϑ including $\vartheta = 0,\pi$ and are otherwise gapped at the threshold field. Away from these lines in $\vartheta - h$, the magnon bands are topologically nontrivial. We further note [47] that the spin-wave spectrum at some ϑ and field $[h - h_{\rm th}(\vartheta)]/S$ is identical to the spectrum at $\vartheta + \pi$ and $[h - h_{\rm th}(\vartheta + \pi)]/S$, where $h_{\rm th}(\vartheta)$ is the threshold field. The band topology is preserved by the mapping so, for example, the ferromagnetic Kitaev point with zero semiclassical threshold field has Chern magnon bands following from results at the $\vartheta = \pi/2$ point.

Finally, to make contact with materials, we observe that in the full J-K-Γ-Γ' nearest-neighbor model of Eq. (1) and Ref. [47] in the fully polarized phase, the linear spin-wave Hamiltonian is related to the Kitaev-Heisenberg model through a mapping of the parameters $J \to J - \Gamma$, $K \to K + \Gamma - \Gamma'$, and $h \to h - 3\Gamma S - 6\Gamma' S$ so topological magnon bands are expected to be present in Kitaev magnets in the paramagnetic regime, at least where spin-wave interactions may be neglected.

Beyond linear spin-wave theory. By expanding in Holstein-Primakoff bosons to order $O(1/S^2)$, one finds three-boson and four-boson terms in the Hamiltonian. The former arise in an expansion around the collinear ground state owing to the anisotropic nature of the exchange. Both the three-body and a subset of the four-body couplings violate particle number conservation and provide a mechanism for the magnons to acquire a finite lifetime. Upon lowering the field, the two magnon states eventually overlap with the single magnon states so that one- to two-magnon decay is kinematically allowed, leading to broadening of the single magnon modes. This process may also lead to the destruction of the chiral edge mode if the widths of the bulk bands or that of the edge mode become comparable to the gap between the magnon bands.

To address the effect of interactions on the bulk spectrum and chiral edge mode we extend the analysis of the previous section in three ways: (i) perturbatively in the magnon-magnon interactions to $O(1/S^2)$ in nonlinear spin-wave theory (NLSWT) [53–57], (ii) nonperturbatively using DMRG with a matrix product operator based time evolution (DMRG+tMPO) [58,59], and (iii) with exact diagonalization (ED) of the Hamiltonian on a 24-site cluster that preserves the lattice symmetries.

First, we examine the dynamical correlation function

$$S(\boldsymbol{k},\omega) \equiv \sum_\alpha S^{\alpha\alpha}(\boldsymbol{k},\omega) = \sum_\alpha \sum_{a,b} \left\langle \mathsf{S}^\alpha_a(-\boldsymbol{k},-\omega)\mathsf{S}^\alpha_b(\boldsymbol{k},\omega)\right\rangle, \tag{3}$$

at the $\vartheta = \pi/2$ point for various fields using linear SWT (LSWT), NLSWT, and DMRG+tMPO. For the latter, the calculations were performed on infinite cylinders with a circumference of eight sites ($L_x = 4$) by a MPO based time evolution of the wave function after a single spin flip is performed on the ground-state wave function. Results at $h = 3$ are shown in Figs. 2(a)–2(c). The DMRG+tMPO, ED, and NLSWT results are in excellent quantitative agreement. At this field, the magnon bands obtained using LSWT remain sharp because the continuum and single magnon modes do not overlap but the upper band is significantly renormalized, presumably because of level repulsion from the two-magnon continuum that has its lower boundary close to the upper magnon branch at this field.

The departure from LSWT predictions becomes more pronounced at lower fields (see SM [47]). At the semiclassical threshold field $h = 2$ ($S = 1/2$) where the lower band condenses across the entire zone, both magnon modes remain gapped and apparently well defined. The upper mode has only a small dispersion at this field and the continuum has a low intensity. The gap closes only at $h \approx 1.25$ for $S = 1/2$. The SM shows corresponding plots for the ferromagnetic Kitaev point, $\vartheta = 3\pi/2$ [47].

To address the fate of the chiral edge modes that are topologically protected within LSWT, we show DMRG+tMPO and NLSWT results for a slab geometry with one periodic direction and two open boundaries. Since the introduction of a boundary destabilizes the fully polarized spin configuration in the vicinity of the edge, LSWT and NLSWT results were obtained by first solving for the noncollinear classical ground state on the slab and perturbing about this solution. All results were obtained for a slab periodic in y with dimensions $L_{\rm x} = 5$ unit cells and length $L_{\rm y} = 71$ for the DMRG chosen to ensure that long enough times could be reached for the requisite energy resolution without entanglement spreading to the y boundaries of the slab.

Figure 3 illustrates dynamical correlations on the slab for the different methods introduced above. The slab geometry is shown in Fig. 3(e) and the different rows [Figs. 3(a)–3(c)] show the k-dependent correlations on different lines through

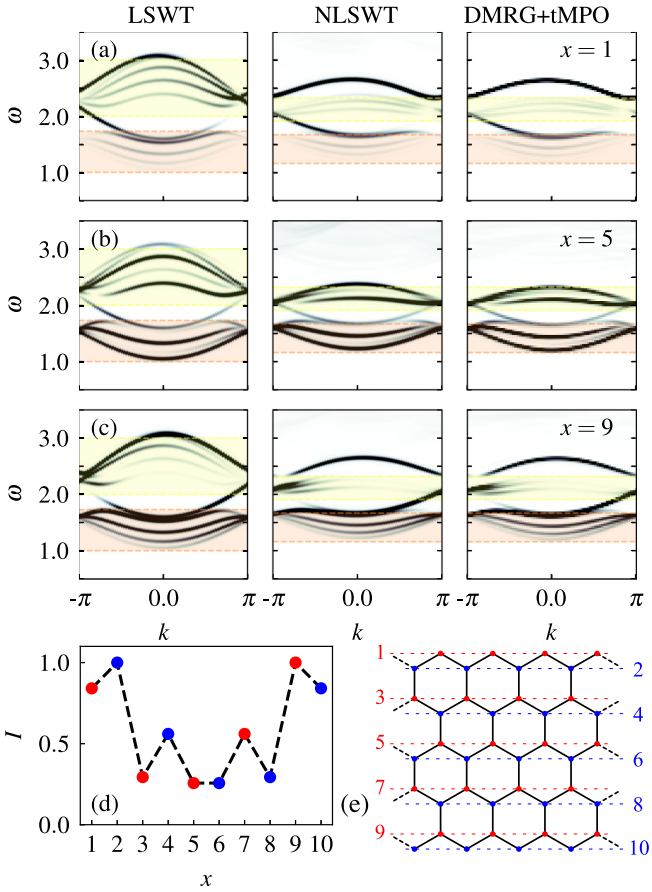

FIG. 3. Dynamical correlation functions $\langle S^x(-k,x,-\omega) S^x(k,x,\omega)\rangle$ computed using DMRG+tMPO (right column) on a slab [illustrated in (e)] of width $L_x = 5$ unit cells and length $L_y = 71$ and with periodic boundary conditions imposed along y. The crystal momentum along the translationally invariant direction is denoted by k and x is the line number [indicated in (e)]. The DMRG+tMPO energy resolution is $\Delta\omega \approx 0.03$. For comparison, corresponding results are shown for linear spin-wave theory (left column) and $O(S^0)$ nonlinear spin-wave theory (middle column). All calculations were performed for $\vartheta = \pi/2$ and $h = 3$. The plots in each row correspond to different line numbers (from top to bottom $x = 1$, 5, and 9). The shading in each figure indicates the bulk single magnon bandwidths with the bulk band gap in between the shaded bands. The chiral modes at the two boundaries $x = 1$ (top) and $x = 9$ (bottom) and their edge character can been seen through the reduction in the band gap intensity in the middle of the slab $x = 5$ (middle) and in (d), which shows the integrated intensity within the bulk band gap in different layers on the slab. The velocities of the edge modes are opposite at the two boundaries.

the slab including the two edges. LSWT for this geometry [Fig. 3 (left column)] shows that the slab is thick enough for the chiral edge modes (which have opposite directions for the two edges) to be well resolved. Figure 3 further shows that the chiral edge modes survive in the full nonperturbative interacting spin model (right) albeit with significant renormalization of the bulk modes, which is almost entirely captured by the interacting spin-wave calculation (middle). Figure 3(d) shows quantitatively that the intensity between the bulk bands is concentrated at the edges.

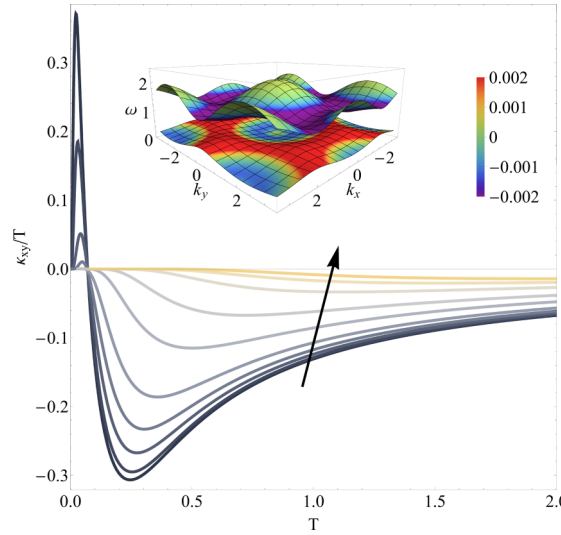

FIG. 4. Dimensionless thermal Hall conductivity κ_{xy}/T as a function of temperature at the ferromagnetic Kitaev point ($S = 1/2$), $K = -1$, at fields $h = 0.01$, 0.02, 0.05, 0.1, 0.2, 0.5, 1, 2, 3, 4 to be read in the arrow direction. The inset shows the dispersions of the bands at $h = 0.1$. The color of the bands indicates the Berry curvature with the scale corresponding to the color bar.

Thermal Hall effect. The presence of a finite Berry curvature in the magnon bands implies the existence of a thermal Hall signature provided that the Berry curvature is not odd in momentum. The magnon thermal Hall effect has been investigated both theoretically and experimentally in a number of magnets [9,13,60–66], including Kitaev magnets [45,67,68]. Earlier theoretical work has explored the thermal Hall response at low fields [69] in the Kitaev honeycomb model. Here, we extend the analysis to Kitaev systems in the high-field regime. Figure 4(b) shows the dimensionless thermal Hall conductivity κ_{xy}/T [47] as a function of temperature and for various magnetic fields at $\vartheta = 3\pi/2$. The shape of the function κ_{xy}/T can be understood as follows. As a function of field, the magnon bands are gapped out, resulting in an exponential decrease in the thermal Hall signature in h. The sign change in κ_{xy} at low temperatures and fields reflects the variation in the Berry curvature in momentum space—the Berry curvature is positive in the vicinity of Γ in the lowest band, this being the maximally thermally occupied state at very low temperatures, while it changes sign for larger momenta. As $T \to \infty$, κ_{xy} saturates to a constant value. It will be interesting to examine recent thermal Hall signatures in α-$RuCl_3$ in light of these results [67].

Discussion. The Hilbert space of a bosonic system encompasses an infinite tower of multiparticle excitations. In insulating magnets, the single magnon sector is meaningful only when the number-nonconserving terms in the magnon Hamiltonian are suppressed, for example, by symmetry, in powers of $1/S$, or when there is a separation of energy scales between the many-magnon states. It is the latter case that we have advocated for in this Rapid Communication as a means of exploring topologically protected magnon edge states. By varying the magnetic field so that the system enters the para-

magnetic phase, the single magnon branches are gapped out and linewidths are suppressed. We have studied the concrete case of spin-orbit coupled honeycomb magnets with significant K, J, Γ, and Γ' terms, finding that the paramagnetic regime generically has Chern magnon bands with chiral edge states. The topological nontriviality is enforced by the anomalous terms in the quadratic Hamiltonian. We anticipate that future experimental developments will facilitate direct measurements of the edge states in such systems.

Note added. Recently, we became aware of Ref. [70], which shows that the ferromagnetic phase of the Kitaev-Heisenberg model has magnon bands with nontrivial Chern number.

K.P. acknowledges Hungarian NKFIH Grant No. K 124176 and support from MPI PKS for an extended stay at the institute during which part of this work was completed. This work was in part supported by the Deutsche Forschungsgemeinschaft under Grant No. SFB 1143.

[1] B. A. Bernevig and T. L. Hughes, *Topological Insulators and Topological Superconductors* (Princeton University Press, Princeton, NJ, 2013).
[2] M. Z. Hasan and C. L. Kane, Rev. Mod. Phys. **82**, 3045 (2010).
[3] B. Yan and C. Felser, Annu. Rev. Condens. Matter Phys. **8**, 337 (2017).
[4] N. P. Armitage, E. J. Mele, and A. Vishwanath, Rev. Mod. Phys. **90**, 015001 (2018).
[5] L. Lu, J. D. Joannopoulos, and M. Soljačić, Nat. Photonics **8**, 821 (2014).
[6] S. H. Mousavi, A. B. Khanikaev, and Z. Wang, Nat. Commun. **6**, 8682 (2015).
[7] P. Delplace, J. B. Marston, and A. Venaille, Science **358**, 1075 (2017).
[8] R. Shindou, R. Matsumoto, S. Murakami, and J.-i. Ohe, Phys. Rev. B **87**, 174427 (2013).
[9] A. Mook, J. Henk, and I. Mertig, Phys. Rev. B **89**, 134409 (2014).
[10] A. Mook, J. Henk, and I. Mertig, Phys. Rev. B **90**, 024412 (2014).
[11] S. A. Owerre, J. Phys.: Condens. Matter **28**, 386001 (2016).
[12] S. A. Owerre, J. Appl. Phys. **121**, 223904 (2017).
[13] J. Romhányi, K. Penc, and R. Ganesh, Nat. Commun. **6**, 6805 (2015).
[14] P. A. McClarty, F. Krüger, T. Guidi, S. F. Parker, K. Refson, A. W. Parker, D. Prabhakaran, and R. Coldea, Nat. Phys. **13**, 736 (2017).
[15] K. Nakata, S. K. Kim, J. Klinovaja, and D. Loss, Phys. Rev. B **96**, 224414 (2017).
[16] R. Chisnell, J. S. Helton, D. E. Freedman, D. K. Singh, R. I. Bewley, D. G. Nocera, and Y. S. Lee, Phys. Rev. Lett. **115**, 147201 (2015).
[17] A. L. Chernyshev and P. A. Maksimov, Phys. Rev. Lett. **117**, 187203 (2016).
[18] S. M. Winter, A. A. Tsirlin, M. Daghofer, J. van den Brink, Y. Singh, P. Gegenwart, and R. Valenti, J. Phys.: Condens. Matter **29**, 493002 (2017).
[19] J. G. Rau, E. K.-H. Lee, and H.-Y. Kee, Annu. Rev. Condens. Matter Phys. **7**, 195 (2016).
[20] S. Trebst, arXiv:1701.07056.
[21] M. Hermanns, I. Kimchi, and J. Knolle, Annu. Rev. Condens. Matter Phys. **9**, 17 (2018).
[22] G. Jackeli and G. Khaliullin, Phys. Rev. Lett. **102**, 017205 (2009).
[23] J. Chaloupka, G. Jackeli, and G. Khaliullin, Phys. Rev. Lett. **105**, 027204 (2010).
[24] S. Choi, R. Coldea, A. Kolmogorov, T. Lancaster, I. Mazin, S. Blundell, P. Radaelli, Y. Singh, P. Gegenwart, K. Choi *et al.*, Phys. Rev. Lett. **108**, 127204 (2012).
[25] Y. Singh and P. Gegenwart, Phys. Rev. B **82**, 064412 (2010).
[26] Y. Singh, S. Manni, J. Reuther, T. Berlijn, R. Thomale, W. Ku, S. Trebst, and P. Gegenwart, Phys. Rev. Lett. **108**, 127203 (2012).
[27] J. Reuther, R. Thomale, and S. Trebst, Phys. Rev. B **84**, 100406 (2011).
[28] F. Ye, S. Chi, H. Cao, B. C. Chakoumakos, J. A. Fernandez-Baca, R. Custelcean, T. F. Qi, O. B. Korneta, and G. Cao, Phys. Rev. B **85**, 180403(R) (2012).
[29] K. W. Plumb, J. P. Clancy, L. J. Sandilands, V. V. Shankar, Y. F. Hu, K. S. Burch, H.-Y. Kee, and Y.-J. Kim, Phys. Rev. B **90**, 041112(R) (2014).
[30] V. M. Katukuri, S. Nishimoto, V. Yushankhai, A. Stoyanova, H. Kandpal, S. Choi, R. Coldea, I. Rousochatzakis, L. Hozoi, and J. van den Brink, New J. Phys. **16**, 013056 (2014).
[31] M. Majumder, M. Schmidt, H. Rosner, A. A. Tsirlin, H. Yasuoka, and M. Baenitz, Phys. Rev. B **91**, 180401(R) (2015).
[32] S. H. Chun, J.-W. Kim, J. Kim, H. Zheng, C. C. Stoumpos, C. Malliakas, J. Mitchell, K. Mehlawat, Y. Singh, Y. Choi *et al.*, Nat. Phys. **11**, 462 (2015).
[33] J. A. Sears, M. Songvilay, K. W. Plumb, J. P. Clancy, Y. Qiu, Y. Zhao, D. Parshall, and Y.-J. Kim, Phys. Rev. B **91**, 144420 (2015).
[34] L. Janssen, E. C. Andrade, and M. Vojta, Phys. Rev. Lett. **117**, 277202 (2016).
[35] L. Janssen, E. C. Andrade, and M. Vojta, Phys. Rev. B **96**, 064430 (2017).
[36] A. Banerjee, C. Bridges, J.-Q. Yan, A. Aczel, L. Li, M. Stone, G. Granroth, M. Lumsden, Y. Yiu, J. Knolle *et al.*, Nat. Mater. **15**, 733 (2016).
[37] S. M. Winter, Y. Li, H. O. Jeschke, and R. Valenti, Phys. Rev. B **93**, 214431 (2016).
[38] S. Williams, R. Johnson, F. Freund, S. Choi, A. Jesche, I. Kimchi, S. Manni, A. Bombardi, P. Manuel, P. Gegenwart *et al.*, Phys. Rev. B **93**, 195158 (2016).
[39] A. Wolter, L. Corredor, L. Janssen, K. Nenkov, S. Schönecker, S.-H. Do, K.-Y. Choi, R. Albrecht, J. Hunger, T. Doert *et al.*, Phys. Rev. B **96**, 041405 (2017).
[40] A. Ponomaryov, E. Schulze, J. Wosnitza, P. Lampen-Kelley, A. Banerjee, J.-Q. Yan, C. Bridges, D. Mandrus, S. Nagler, A. Kolezhuk *et al.*, Phys. Rev. B **96**, 241107 (2017).
[41] S. M. Winter, K. Riedl, P. A. Maksimov, A. L. Chernyshev, A. Honecker, and R. Valentí, Nat. Commun. **8**, 1152 (2017).
[42] S.-H. Baek, S.-H. Do, K.-Y. Choi, Y. S. Kwon, A. U. B. Wolter, S. Nishimoto, J. van den Brink, and B. Büchner, Phys. Rev. Lett. **119**, 037201 (2017).
[43] J. A. Sears, Y. Zhao, Z. Xu, J. W. Lynn, and Y.-J. Kim, Phys. Rev. B **95**, 180411(R) (2017).
[44] A. Kitaev, Ann. Phys. **321**, 2 (2006).

[45] Y. Kasahara, T. Ohnishi, Y. Mizukami, O. Tanaka, S. Ma, K. Sugii, N. Kurita, H. Tanaka, J. Nasu, Y. Motome, T. Shibauchi, and Y. Matsuda, Nature **559**, 227 (2018).
[46] J. G. Rau, E. K.-H. Lee, and H.-Y. Kee, Phys. Rev. Lett. **112**, 077204 (2014).
[47] See Supplemental Material at http://link.aps.org/supplemental/10.1103/PhysRevB.98.060404 for further information on the exchange model, the linear and interacting spin wave theory, thermal Hall effect, the DMRG method and additional spin wave spectra.
[48] A. Little, L. Wu, P. Lampen-Kelley, A. Banerjee, S. Pantankar, D. Rees, C. A. Bridges, J.-Q. Yan, D. Mandrus, S. E. Nagler *et al.*, Phys. Rev. Lett. **119**, 227201 (2017).
[49] Z. Wang, S. Reschke, D. Hüvonen, S.-H. Do, K.-Y. Choi, M. Gensch, U. Nagel, T. Rõõm, and A. Loidl, Phys. Rev. Lett. **119**, 227202 (2017).
[50] K. Ran, J. Wang, W. Wang, Z.-Y. Dong, X. Ren, S. Bao, S. Li, Z. Ma, Y. Gan, Y. Zhang *et al.*, Phys. Rev. Lett. **118**, 107203 (2017).
[51] T. Holstein and H. Primakoff, Phys. Rev. **58**, 1098 (1940).
[52] Physical time reversal can be broken by magnetic order or by an external magnetic field. For our purposes one must ask whether there is some antiunitary operator $\mathcal{T} \equiv U_T K$ that acts on the Hamiltonian such that $U_T^\dagger \mathbf{M}^\star(\boldsymbol{k}) U_T = \mathbf{M}(-\boldsymbol{k})$. For the $\vartheta = 0$ model the unitary operator U_T acts trivially and the tight-binding model has an effective time-reversal symmetry. This is broken by the anomalous terms when the Kitaev term is switched on.
[53] J.-P. Blaizot and G. Ripka, *Quantum Theory of Finite Systems* (MIT Press, Cambridge, MA, 1986), Vol. 3.
[54] A. Chubukov, S. Sachdev, and T. Senthil, J. Phys.: Condens. Matter **6**, 8891 (1994).
[55] A. L. Chernyshev and M. E. Zhitomirsky, Phys. Rev. B **79**, 144416 (2009).
[56] M. Mourigal, W. T. Fuhrman, A. L. Chernyshev, and M. E. Zhitomirsky, Phys. Rev. B **88**, 094407 (2013).
[57] M. E. Zhitomirsky and A. L. Chernyshev, Rev. Mod. Phys. **85**, 219 (2013).
[58] M. Gohlke, R. Verresen, R. Moessner, and F. Pollmann, Phys. Rev. Lett. **119**, 157203 (2017).
[59] M. P. Zaletel, R. S. K. Mong, C. Karrasch, J. E. Moore, and F. Pollmann, Phys. Rev. B **91**, 165112 (2015).
[60] H. Katsura, N. Nagaosa, and P. A. Lee, Phys. Rev. Lett. **104**, 066403 (2010).
[61] R. Matsumoto and S. Murakami, Phys. Rev. B **84**, 184406 (2011).
[62] R. Matsumoto, R. Shindou, and S. Murakami, Phys. Rev. B **89**, 054420 (2014).
[63] Y. Onose, T. Ideue, H. Katsura, Y. Shiomi, N. Nagaosa, and Y. Tokura, Science **329**, 297 (2010).
[64] T. Ideue, Y. Onose, H. Katsura, Y. Shiomi, S. Ishiwata, N. Nagaosa, and Y. Tokura, Phys. Rev. B **85**, 134411 (2012).
[65] S. Murakami and A. Okamoto, J. Phys. Soc. Jpn. **86**, 011010 (2016).
[66] D. Watanabe, K. Sugii, M. Shimozawa, Y. Suzuki, T. Yajima, H. Ishikawa, Z. Hiroi, T. Shibauchi, Y. Matsuda, and M. Yamashita, Proc. Natl. Acad. Sci. USA **113**, 8653 (2016).
[67] Y. Kasahara, K. Sugii, T. Ohnishi, M. Shimozawa, M. Yamashita, N. Kurita, H. Tanaka, J. Nasu, Y. Motome, T. Shibauchi, and Y. Matsuda, Phys. Rev. Lett. **120**, 217205 (2018).
[68] R. Hentrich, M. Roslova, A. Isaeva, T. Doert, W. Brenig, B. Büchner, and C. Hess, arXiv:1803.08162.
[69] J. Nasu, J. Yoshitake, and Y. Motome, Phys. Rev. Lett. **119**, 127204 (2017).
[70] D. G. Joshi, Phys. Rev. B **98**, 060405 (2018).